High Temperature Reaction of S + SO_2 → SO + SO: Implication of S_2O_2 Intermediate Complex Formation

Yoshinori Murakami,*,† Shouichi Onishi,† Takaomi Kobayashi,† Nobuyuki Fujii,† Nobuyasu Isshiki,§ Kentaro Tsuchiya,‡ Atsumu Tezaki,§ and Hiroyuki Matsui||

Department of Chemistry, Nagaoka University of Technology, Niigata 940-2188, Japan, National Institute of Advanced Industrial Science and Technology, Ibaraki 305-8569, Japan, Department of Mechanical Engineering, The University of Tokyo, Tokyo 113-8656, Japan, and Department of Ecological Engineering, Toyohashi University of Technology, Toyohashi 441-8580, Japan

Received: April 21, 2003; In Final Form: August 28, 2003

The rate constant for the reaction S + SO_2 → SO + SO (1) has been investigated by measuring time profiles of S atoms behind reflected shock waves using two experimental systems: S atoms were provided by the thermal decomposition of COS in the high-temperature range (2020−2800 K) and by excimer laser photolysis of COS in the low-temperature range (T = 1120−1540 K). The results of these experiments yield the rate constant with a non-Arrhenus temperature dependence, $k_1 = 10^{-39.73}T^{8.21}\exp(4828.5/T)$ cm^3 molecules^{-1} s^{-1}, over the extended temperature range (1120−2800 K). By comparing the rate constants with that derived from a conventional transition-state theory based on the potential energy surface calculated by the G2M-(CC1) methodology, a reaction mechanism including a contribution of the singlet state of the reaction intermediate S_2O_2 is discussed.

Introduction

Low-quality fuels that contain a large quantity of sulfur are used in a variety of combustion systems. Since the fuel sulfur has profound effects on the overall flame characteristics (i.e. NO_x formation,[1] soot formation,[2,3] flame temperature[4]), modeling studies in sulfur-containing flames have been carried out by several authors.[5−8] Recently, kinetic studies related to sulfur-containing species have been extensively conducted at high-temperature ranges; thus, an improved kinetic database to model sulfur-containing flames is now available.[9] Despite such progress, there still remain key elementary reactions which are not well explored. For example, only limited kinetic works have been performed for reactions of SO_2 with atoms or radicals, which can potentially play key roles in the formation of reduced sulfur species such as H_2S and S_2 in the postflame regions of H_2/O_2 and hydrocarbon/O_2 flames doped with SO_2.[7,8,10] In accordance with such requirements, an investigation for the reaction

$$S + SO_2 \rightarrow SO + SO \qquad (1)$$

is the issue of this study. Reaction 1 is believed to play an important role in the conversion between SO and SO_2 at flame temperature under fuel-rich conditions. However, to our knowledge, only an estimation by Just and Rimpel[11] is available in the database, and no direct experimental investigation has been performed at high temperatures above 1000 K. The reverse reaction

$$SO + SO \rightarrow SO_2 + S \qquad (-1)$$

was investigated by several authors at room temperature;[12−15] however, the activation energy for (−1) was not given, so that the kinetic information at flame temperature is not available.

In this work, the title reaction 1 was investigated by measuring time profiles of S atoms with atomic resonance absorption spectrometry (ARAS) behind reflected shock waves in COS/SO_2/Ar mixtures. Two types of shock tube experiment were conducted; that is, S atoms were produced by thermal decomposition of COS at a high-temperature range between 2020 and 2800 K, or in contrast, an excimer laser photolysis shock tube technique was employed to cover the lower temperature range between 1120 and 1540 K. The measurements indicate a slight non-Arrhenius temperature dependence of the rate constant over the extended temperature range.

To examine the reaction mechanism, ab initio calculations were carried out to evaluate the potential energies of the reaction intermediates including triplet and singlet states, and the discussion of the reaction mechanism is supplied.

Experimental Section

Two different shock tube systems were employed to measure the rate constant for reaction 1. In both systems, S atoms were monitored by using ARAS behind the reflected shock waves in COS/SO_2/Ar mixtures. At Nagaoka University of Technology (NUT), S atoms were produced by the thermal decomposition of COS in a diaphragmless shock tube having a driven section of 3.5 m long and 46 mm i.d. At the University of Tokyo (UT), S atoms were produced by KrF excimer laser photolysis (Lambda Phisik LPX100: λ = 248 nm) of COS by using a diaphragmless shock tube having a driven section of 4 m long with 40 mm i.d. Laser radiation was sent at about 100 μs after the arrival of a reflected shock wave at the observation section through a quartz window placed at the end plate of the shock tube. The typical fluence of the laser pulse was 60 mJ/cm^2 at the front of the entrance window. O atoms were also monitored in the experiment at UT.

* To whom correspondence should be addressed.
† Nagaoka University of Technology.
‡ National Institute of Advanced Industrial Science and Technology.
§ The University of Tokyo.
|| Toyohashi University of Technology.

10.1021/jp030471i CCC: $25.00
Published on Web 11/22/2003

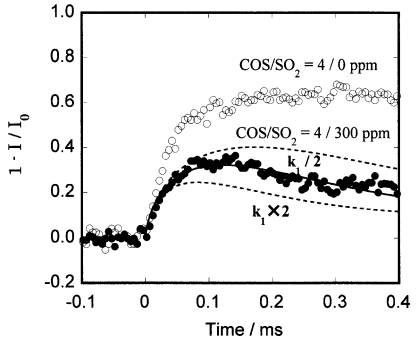

Figure 1. Examples showing the time dependences of the S atom produced in the thermal decomposition of COS measured at NUT. Experimental results: ○, COS/SO_2 = 4/0 ppm; ●, COS/SO_2 = 4/300 ppm. Calculated profiles: solid curve, k_1 given by (I) in the text; dotted curves, k_1 factored by 2 or $^1/_2$, T = 2500 K, P = 1.3 atm.

The ARAS systems both at NUT and UT consisted of a microwave-discharge lamp, a vacuum UV monochromator (Ritsu MCV-20), and a solar blind photomultiplier (Hamamatsu R-1080, R-976). Perpendicular to the optical axis of the ARAS system, a piezoelectric transducer was equipped to monitor the pressure profiles at the observation area. The atomic resonance emission of S atoms was produced by microwave discharge of He containing 0.1% SO_2 or 0.2% H_2S mixtures. Absorption intensity was recorded and stored in an oscilloscope and sent to a personal computer for analysis. To obtain the relation between the measured absorption at λ = 182 nm (S atomic line) and the corresponding S atom concentrations, high-temperature dissociation of COS and CS_2 was used. Sample gases (SO_2 and COS) were purified by the freeze-and-thaw method. Ar (CP grade) was used without further purification.

Experimental Results

In the experiment at NUT, the concentration of COS was kept less than 2 × 10^{13} molecule cm^{-3} behind the reflected shock waves to avoid the secondary reaction S + COS → CO + S_2. Typical examples of the time profile of the S atom with and without coexistence of SO_2 are shown in Figure 1. These traces show a rise at first due to the thermal decomposition of COS, that is,

$$\mathrm{COS + Ar \rightarrow CO + S + Ar} \qquad (2)$$

Since the time profile of S atom absorption showed no appreciable decay behind the reflected shock of COS/Ar mixtures, it was confirmed that subsequent reactions that consume S atoms such as

$$\mathrm{S + COS \rightarrow CO + S_2} \qquad (3)$$

were negligible: this conclusion was further confirmed by conducting kinetic simulations using the rate constant for reaction 3 determined previously by Oya et al.[16]

In contrast, time profiles of S atoms with addition of SO_2 show clear decay following an initial rise. The decay rate showed a linear correlation with the concentration of SO_2. Therefore, it is reasonable to conclude that this decay is in part due to the title reaction 1. The rate constant for (1) was determined by fitting the observed time profiles of S atoms in the COS/SO_2/Ar mixtures with those obtained by kinetic simulations. Since the concentration of COS was low enough, only (1) and (2) should be taken into account for the present analyses. The calculated profiles are compared with the experimental traces in Figure 1. From these kinetic analyses, the rate constants for reaction 1 were determined and the results are summarized in Figure 2.

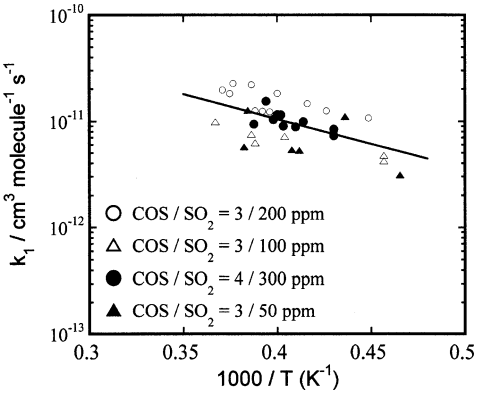

Figure 2. Arrhenius plot for the reaction rate of S + SO_2 → SO + SO (1) obtained at NUT. Solid line: The least-squares fit to the present data.

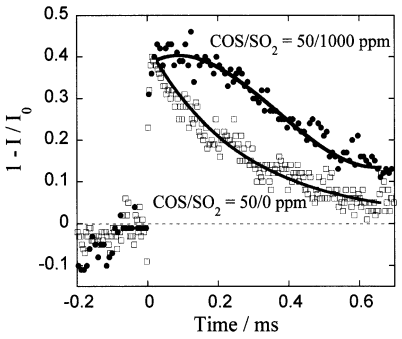

Figure 3. Examples showing the time dependences of the S atom produced in the laser flash photolysis of COS measured at UT. Experimental results: □, COS/SO_2 = 50/0 ppm; ●, COS/SO_2 = 50/1000 ppm. Calculated profiles: solid curves, k_1 given by (II) in the text, T = 1600 K, P = 1.4 atm.

From a simple least-squares analysis, the Arrhenius expression for this reaction rate is given by

$$k_1 = 10^{-9.10\pm0.65} \exp(-89.8 \pm 30.6\ \mathrm{kJ}/RT)\ \mathrm{cm^3\,molecules^{-1}\,s^{-1}} \qquad (\mathrm{I})$$

over the temperature range between 2020 and 2800 K.

In the experiment at UT, an excimer laser flash photolysis shock tube technique was used to determine the rate constant for the lower temperature range from 1120 to 1540 K. Figure 3 shows typical examples of the time profiles of S atoms in the photolysis of COS with and without addition of SO_2. In the case without SO_2, S atoms were instantly produced by the flash photolysis of COS and then simply decayed. The decay rate was confirmed to be in good agreement with the previous results[16,17] for reaction 3. In the case with a large excess of SO_2, S atoms show an initial increase (as is shown in Figure 3), followed by a slower decay. Since intense irradiation from the KrF excimer laser yields O atoms, reactions of O atoms with COS and SO_2 should be considered[18] in this study, that is,

$$\mathrm{O + COS \rightarrow products} \qquad (4)$$

$$\mathrm{O + SO_2 \rightarrow SO + O_2} \qquad (5)$$

Reliable rate constants are available for reactions 2−5; however, it was confirmed that two main product channels

$$\mathrm{O + COS \rightarrow CO_2 + S} \qquad (4a)$$

$$\mathrm{O + COS \rightarrow S + CO_2} \qquad (4b)$$

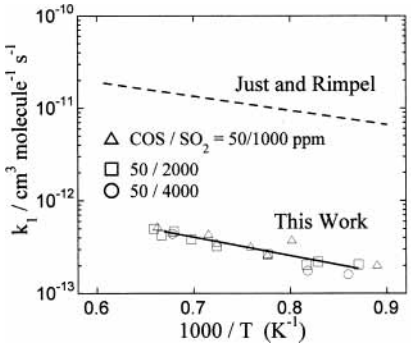

Figure 4. Arrhenius plot for the reaction of S + SO_2 → SO + SO determined by an excimer laser photolysis shock tube technique at UT. The solid line is the least-squares fit to the present data, and the dashed line is the fit to the data of Just and Rimpel.[11]

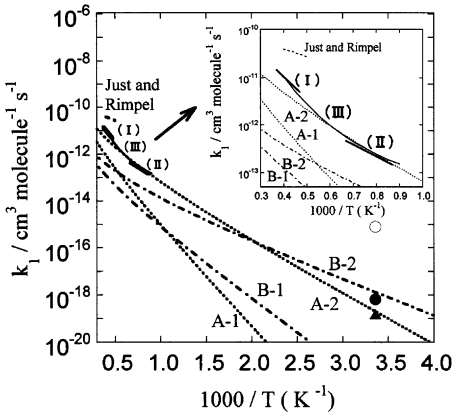

Figure 5. Comparison of the experimental and theoretical rate constants for the S + SO_2 reaction 1. Solid curves: Present experimental results. (I): The result at NUT. (II): The result at UT. (III): Summary of (I) and (II), given in the text as (III). Dashed line: Just and Rimpel.[11] Dotted lines: Calculated rate constants, assuming that the reaction proceeds fully in the triplet surface (case A) with a varying barrier height (E_0) of TS1. [A-1: $E_0 = 75$. A-2: $E_0 = 40$ kJ mol^{-1}.] Dashed−dotted lines: Calculated limiting rate constants assuming that the reaction is carried out by a triplet to singlet intersystem crossing followed by passage through TS5 (case-B). [B-1: $E_0 = 53$. B-2: $E_0 = 30$ kJ mol^{-1}.] Rate constants at room temperature are calculated using the rate constants of the reverse reaction SO + SO → SO_2 + S given in ref 13 (●), ref 14 (▲), and ref 15 (○).

exist in reaction 4.[18] By adjusting the magnitude of the rate constant for reaction 1 as well as the branching fraction for (4b), the observed time profiles for S and O atoms can be well reproduced by a kinetic simulation with reactions 1−5. An example of such a comparison is shown in Figure 3 only for the profile of the S atom. More details in these analyses are presented elsewhere.[18] As a result, the rate constant for reaction 1 is given by

$$k_1 = 10^{-11.01\pm0.33} \exp(-37.8 \pm 8.2 \text{ kJ mol}^{-1}/RT) \text{ cm}^3 \text{ molecule}^{-1} \text{ s}^{-1} \quad \text{(II)}$$

for the temperature range between 1120 and 1540 K. The resultant Arrhenius plot is shown in Figure 4.

The rate constants for reaction 1 obtained by using two different techniques are summarized in Figure 5. The rate constant for reaction 1 at room temperature is also included in Figure 5 by combining the previous results[13−15] on the rate constants for the reverse reaction SO + SO → SO_2 + S and the equilibrium constant from the standard enthalpy and entropy of this reaction. As shown in the figure, the rate constant obtained in the present work is about $^1/_3$ of that estimated by Just and Rimpel[11] at the overlapping temperature range. Just and Rimpel[11] measured O atoms behind the reflected shock of SO_2 highly diluted with Ar mixtures and discussed the rate constant for the decomposition of SO_2 at high temperature. To investigate the influence of the subsequent reactions on the time profiles of O atoms behind the shock of SO_2/Ar mixtures, they used the estimated rate constant for the reaction S + SO_2 → SO + SO as one of the subsequent reactions. Since this estimated rate constant has little or no influence on the time profiles of O atoms, the more straightforward method used in this work probably gave correct values for the rate constant of reaction 1. Combining the rate constants obtained in this study over an extended temperature range between 1120 and 2800 K, a nonlinear least-squares analysis gives a non-Arrhenius behavior of the rate constant expressed as

$$k_1 = 10^{-39.73} T^{8.21} \exp(4828.5/T) \text{ cm}^3 \text{ molecule}^{-1} \text{ s}^{-1} \quad \text{(III)}$$

Discussions on PES of Reaction Pathways

To examine the observed non-Arrhenius behavior of the rate constant for reaction 1, ab initio molecular orbital calculations were carried out. Gaussian 98[19] and Molpro 2000[20] codes were used for the PES calculations for the singlet and triplet S + SO_2 system. All minima and transition states (TS) were optimized using the B3LYP hybrid density functional method[21,22] and the aug-cc-pVTZ+1 basis set.[23] G2M (CC1) calculations[24] were performed at the B3LYP/aug-cc-pVTZ+1 optimized geometry in order to determine more accurate energies. No stable wave functions for a pure spin state have been found for a few intermediates and transition states on the singlet surface (at the hybrid density functional calculations), even though there is no lower lying triplet state than the singlet. In such a case the optimization of geometry was conducted allowing spin contamination. Since the G2M procedures were inevitably performed for a wave function of a pure spin state, the G2M energies thus obtained may be considerably uncertain.

Results of the PES calculations are illustrated in Figure 6, where triplet surfaces are represented by solid lines and singlet surfaces by dashed lines. Rotational constants and vibration frequencies of several minima and transition states are summarized in Table 1. On the triplet surfaces, S(^{3}P) + SO_2 correlates to ^{3}SOSO by passage through TS1 and/or TS2. ^{3}SOSO has two conformers: one nonplanar and the other planar trans-type (^{3}A′), which correlate to OSSO(^{3}B) via TS3. Both ^{3}SOSO and ^{3}OSSO dissociate to ^{3}SO + ^{3}SO without an explicit potential barrier beyond the endothermicity. Besides these intermediates, there is an unstable adduct, SSO_2(^{3}A"), only slightly higher in energy than the level of S + SO_2.

There were found four intermediates in the singlet reaction courses to ^{3}SO + ^{3}SO. Planar $^1SSO_2$, an analogue of sulfur trioxide, connected with ^{1}S + SO_2 has the lowest energy in the system. By the halfway migration of the end S atom through TS5, $^1SSO_2$ correlates to ^{1}SOS═O, which has a three-membered ring structure. ^{1}SOS═O correlates to ^{1}SOSO and ^{1}OSSO (having two conformers, planar cis- and trans-type, respectively), which are predicted to be more stable than the corresponding triplet states. The two conformers of ^{1}SOSO, however, have no stable wave function for a pure spin state. For ^{1}OSSO, a stable wave function for a pure spin state is not obtained for the trans-type conformer whereas it is obtained for the cis-type one. This kind of instability is perhaps due to a biradical character of these intermediates. It is estimated that ^{1}SOSO correlates to ^{3}SO + ^{3}SO with an appreciable intervening barrier, whereas ^{1}OSSO has no barrier.

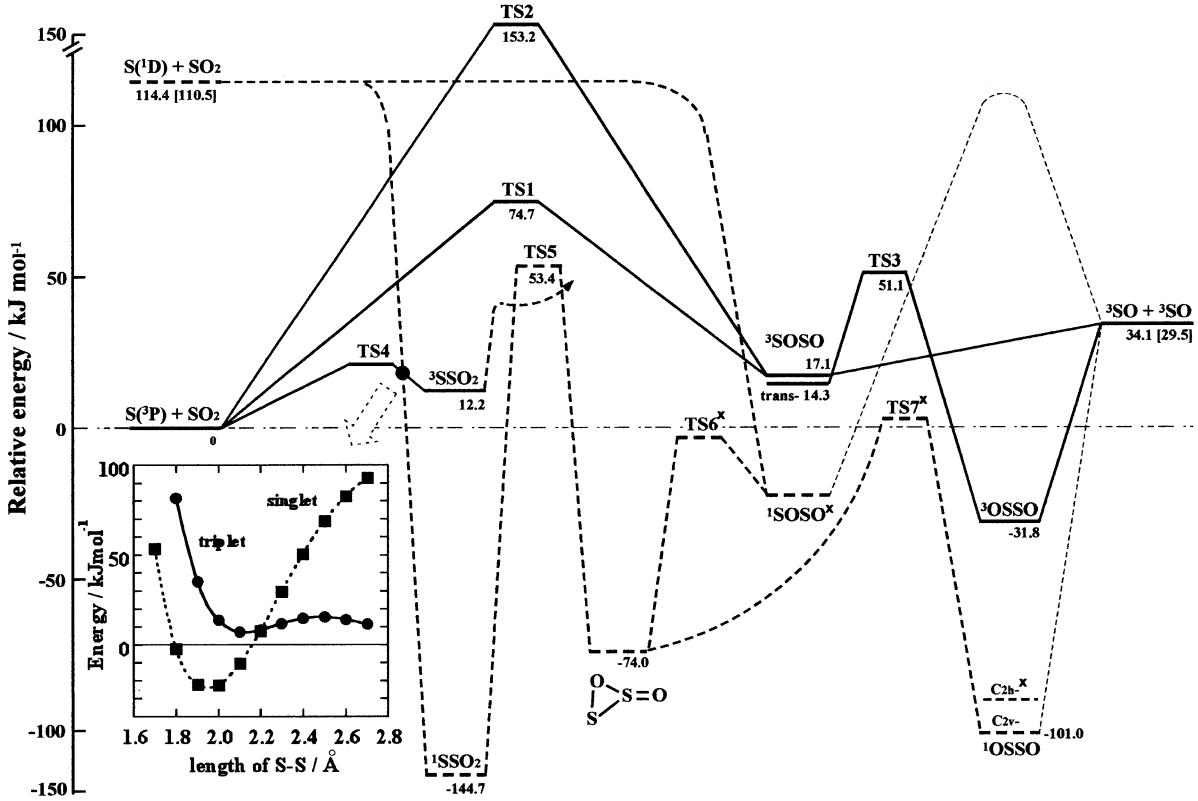

Figure 6. Potential energy diagram of the S + SO_2 system calculated at the G2M(CC1)//B3LYP/aug-cc-pVTZ+1 level: solid lines, triplet; dashed lines, singlet; lighter lines are estimates. Figures in parentheses denote the experimental values. An x on the right shoulder represents that no stable wave function for a pure spin state was obtained in the B3LYP calculations (see text). Energies are given relative to S(^{3}P) + SO_2, including ZPE. Inset: potential energy (not including ZPE) of singlet SSO_2 at the partially optimized geometry of triplet SSO_2 (^{3}A"), which constrained the length of the S−S bond.

TABLE 1: Rotational Constants and Vibrational Frequencies of SO_2, SO, Intermediates, and Transition States in the S + SO_2 System

	rotational constants/GHz			vibrational frequencies/cm^{-1}						ZPE[a]/(kJ mol^{-1})
SO_2	59.6	10.3	8.76				519	1177	1374	18.4
^{3}SO	21.4	21.4							1157	6.9
TS1	15.9	2.35	2.15	527i	107	187	480	786	1234	16.7
TS2	13.1	3.42	3.11	1209i	148	365	386	712	1225	17.0
nonplanar-^{3}SOSO	15.2	2.79	2.49	76	209	401	561	758	1180	19.0
trans-^{3}SOSO (^{3}A′)	31.4	2.38	2.21	57	188	325	623	811	1195	19.1
TS3 (^{3}A′)	26.4	2.18	2.01	164i	109	218	463	986	1194	17.8
^{3}OSSO (^{3}B)	13.8	2.71	2.58	87	198	266	362	1053	1095	18.3
$^3SSO_2$ (^{3}A")	9.16	3.94	2.88	143	248	419	480	1086	1279	21.9
$^1SSO_2$ ($^1A_1$)	10.3	4.36	3.06	345	404	468	665	1176	1368	26.5
TS5	10.3	4.01	3.06	625i	256	375	463	1025	1289	20.4
^{1}SOS═O	13.3	3.89	3.46	267	415	443	562	807	1269	22.5
cis-^{1}OSSO ($^1A_1$)	13.4	3.35	2.68	138	285	476	492	1138	1191	22.2

[a] The values of ZPE were calculated with the scaling factor 0.985.

Singlet and triplet potential energy surfaces in the system seem to intersect in a complicated manner. Although exploring the seam of crossing is beyond the present ab initio calculations, a crossing point was found for a geometry around $^3SSO_2$, where the energy of $^1SSO_2$ increases to the level of the triplet state due to the shift of the end S atom from the molecular plane and the stretch of the S−S bond distance. This is shown in the inset of Figure 6.

According to the results of the PES calculations, the magnitude of the potential barrier in the triplet reaction is considerably larger than the observed activation energy in the present experiments. Apart from an inefficient triplet/singlet transition, a reaction course via the intersystem crossing followed by passage through TS5 is more favorable energetically than those through fully triplet channels. To examine the reaction course(s) of S(^{3}P) + SO_2, we calculated rate constants on the basis of a conventional transition-state theory (TST), with vibrational frequencies and rotational constants obtained by the B3LYP method and the G2M(CC1) energy in hand. Wigner's tunneling correction was also included.

(Case A) Reaction Pathways along the Triplet Surfaces. If the reaction proceeds only on the triplet surface, derived rate constants with the potential barrier (E_0) of 75 kJ mol^{-1} in TS1 are much lower than the experimental values, as is shown in Figure 5. Since the most important error in the TST calculations was expected to be the barrier height, calculated rate constants with reduced values of E_0 were compared with the experimental ones in the same figure. Although a perfect correspondence between the present theoretical and experimental rate constants is not possible, a value of E_0 = 40 kJ mol^{-1} gives acceptable agreement with the present experimental values at the lower temperatures. This corresponds to a potential barrier of 10 kJ

mol^{-1} for the reverse reaction, $^3SO + {}^3SO \rightarrow {}^3S + SO_2$ (−1). With this value, the rate constant for (−1) is estimated as 4.5×10^{-15} cm^3 $molecule^{-1}$ s^{-1} at room temperature: this value is more or less consistent with the reported values of 3.5×10^{-15} and 8.3×10^{-16} cm^3 $molecule^{-1}$ s^{-1},[13,14] but it is inconsistent with the reported value of 4.3×10^{-12} cm^3 $molecule^{-1}$ s^{-1}. [15]

(Case B) Reaction Pathways with Triplet to Singlet Intersystem Crossing. If the $S(^3P) + SO_2$ reaction was assumed to be carried out by the triplet to singlet intersystem crossing followed by passage through TS5, the bottlenecks for the reaction are inefficient triplet/singlet transition and/or the height of the potential barrier in TS5. Assuming the triplet/singlet transition probability is near unity, we can calculate the upper limit of the rate constant using the information on TS5. As is shown by dashed dotted lines in Figure 5, derived limiting rate constants are markedly smaller than those from experiments even if the barrier height is reduced from 53 to 30 kJ mol^{-1}, which is a lower limit arising from the endothermicity. Also, the calculated rate constants are much smaller than those from the fully triplet reaction course via TS1 even though both have the same magnitude of activation energy. This is mainly due to the larger contribution of the vibrational partition function with low frequencies in the looser TS1 than those in TS5.

Although these TST calculations suggest that the G2M (CC1) methodology considerably overestimates the height of the potential barriers of TS1 and also that these calculations could not completely explain the non-Arrhenius behavior of the rate constant, it is reasonable to conclude that the $S(^3P) + SO_2$ reaction proceeds fully on the triplet surfaces via S_2O_2 complex intermediates leading to SO molecules as end products.

Conclusions

This work supplies the results of the first measurements of the rate constant for the reaction $S + SO_2 \rightarrow SO + SO$ over the temperature range 1120−2800 K. Slight non-Arrhenius behavior of the rate constant for this reaction is indicated. The rate constant based on ab initio calculations of potential energy surfaces for this reaction along with a conventional transition state theory cannot explain the present experimental observations, however, it is indicated that the reaction proceeds only with triplet surfaces via the intermediate complex S_2O_2.

References and Notes

(1) Cortley, T. L.; Wendy, J. O. L. *Combust. Flame* **1984**, *58*, 141.
(2) Lawton, S. A. *Combust. Flame* **1989**, *75*, 175.
(3) Gulder, O. L. *Combust. Flame* **1993**, *92*, 410.
(4) Kallend, A. S. *Combust. Flame* **1972**, *19*, 227.
(5) Smith, O. I.; Wang, S. N.; Tseregounis, S.; Westbrook, C. K. *Combust. Sci. Technol.* **1983**, *30*, 241.
(6) Wendt, J. O. L.; Wootan, J. T. E. C.; Corley, T. L. *Combust. Flame* **1983**, *49*, 261.
(7) Zachariah, M. R.; Smith, O. I. *Combust. Flame* **1987**, *69*, 125.
(8) Glaborg, P.; Kubel, D.; Dam-Johansen, K.; Chiang, H. M.; Bozelli, J. W. *Int. J. Chem. Kinet.* **1996**, *28*, 773.
(9) Gardiner, W. C. *Gas-Phase Combustion Chemistry*; Springer-Verlag: New York, 2000.
(10) Radi, P. P.; Mischeler, B.; Schlegel, A.; Tzannis, A. P.; Beaud, P.; Gerber, T. *Combust. Flame* **1999**, *118*, 301.
(11) Just, T.; Rimpel, G. *Proceedings of the 11th International Symposium on shock Tubes and Shock Waves*, University of Washinton, Seattle; 1977; p 226.
(12) Herron, J. T.; Huie, R. E. *Chem. Phys. Lett.* **1980**, *76*, 322.
(13) Martinez, R. I.; Herron, J. T. *Int. J. Chem. Kinet.* **1983**, *15*, 1127.
(14) Chung, K.; Calvert, J. G.; Bottenheim, J. W. *Int. J. Chem. Kinet.* **1975**, *7*, 161.
(15) Sullivan, J. O.; Warneck, P. *Ber. Bunsen-Ges. Phys. Chem.* **1965**, *69*, 7.
(16) Oya, M.; Shiina, H.; Tsuchiya, K.; Matsui, H. *Bull. Chem. Soc. Jpn.* **1994**, *67*, 2311.
(17) Woiki, D.; Markus, W.; Roth, P. *J. Phys. Chem.* **1993**, *97*, 9682.
(18) Isshiki, N.; Murakami, Y.; Tsuchiya, K.; Tezaki, A.; Matsui, H. *J. Phys. Chem.* **2003**, *107*, 2464.
(19) Frisch, M. J.; Trucks, G. W.; Schlegel, H. B.; Scuseria, G. E.; Robb, M. A.; Cheeseman, J. R.; Zakrzewski, V. G.; Montgomery, J. A., Jr.; Stratmann, R. E.; Burant, J. C.; Dapprich, S.; Millam, J. M.; Daniels, A. D.; Kudin, K. N.; Strain, M. C.; Farkas, O.; Tomasi, J.; Barone, V.; Cossi, M.; Cammi, R.; Mennucci, B.; Pomelli, C.; Adamo, C.; Clifford, S.; Ochterski, J.; Petersson, G. A.; Ayala, P. Y.; Cui, Q.; Morokuma, K.; Malick, D. K.; Rabuck, A. D.; Raghavachari, K.; Foresman, J. B.; Cioslowski, J.; Ortiz, J. V.; Baboul, A. G.; Stefanov, B. B.; Liu, G.; Liashenko, A.; Piskorz, P.; Komaromi, I.; Gomperts, R.; Martin, R. L.; Fox, D. J.; Keith, T.; Al-Laham, M. A.; Peng, C. Y.; Nanayakkara, A.; Challacombe, M.; Gill, P. M. W.; Johnson, B.; Chen, W.; Wong, M. W.; Andres, J. L.; Gonzalez, C.; Head-Gordon, M.; Replogle, E. S.; Pople, J. A. *Gaussian 98*, revision A.9; Gaussian, Inc.: Pittsburgh, PA, 1998.
(20) MOLPRO is a package of ab initio programs written by Werner, H.-J., and Knowles, P. J., with contributions from Amos, R. D.; Bernhardsson, A.; Berning, A.; Celani, P.; Cooper, D. L.; Deegan, M. J. O.; Dobbyn, A. J.; Eckert, F.; Hampel, C.; Hetzer, G.; Korona, T.; Lindh, R.; Lloyd, A. W.; McNicholas, S. J.; Manby, F. R.; Meyer, W.; Mura, M. E.; Nicklass, A.; Palmieri, P.; Pitzer, R.; Rauhut, G.; Schütz, M.; Stoll, H.; Stone, A. J.; Tarroni, R.; and Thorsteinsson, T.
(21) Becke, A. D. *J. Chem. Phys.* **1993**, *98*, 5648.
(22) Lee, C.; Yang, W.; Parr, R. G. *Phys. Rev. B* **1988**, *37*, 785.
(23) Martin, J. M. L.; de Oliveira, G. *J. Chem. Phys.* **1999**, *111*, 1843.
(24) Mebel, A. M.; Morokuma, K.; Lin, M. C. *J. Chem. Phys.* **1995**, *103*, 7414.